A measurement system for vertical seawater profiles close to the air/sea interface

Richard P. Sims[1,2], Ute. Schuster[2], Andrew. J. Watson[2], Ming Xi. Yang[1], Frances. E. Hopkins[1], John. Stephens[1] and Thomas. G. Bell[1,*]

[1]{Plymouth Marine Laboratory, Plymouth, United Kingdom}

[2]{University of Exeter, Exeter, United Kingdom}

Correspondence to: T. Bell (tbe@pml.ac.uk)

Abstract

This paper describes a Near Surface Ocean Profiler, which has been designed to precisely measure vertical gradients in the top 10 m of the ocean. Variations in the depth of seawater collection are minimised when using the profiler compared to conventional CTD/rosette deployments. The profiler consists of a remotely operated winch mounted on a tethered yet free floating buoy, which is used to raise and lower a small frame housing sensors and inlet tubing. Seawater at the inlet depth is pumped back to the ship for analysis. The profiler can be used to make continuous vertical profiles or to target a series of discrete depths. The profiler has been successfully deployed during wind speeds up to 10 m s^{-1} and significant wave heights up to 2 m. We demonstrate the potential of the profiler by presenting measured vertical profiles of the trace gases carbon dioxide and dimethylsulfide. Trace gas measurements use an efficient microporous membrane equilibrator to minimise the system response time. The example profiles show vertical gradients in the upper 5 m for temperature, carbon dioxide and dimethylsulfide of 0.15 °C, 4 µatm and 0.4 nM respectively.

1 Introduction

Exchange between the ocean and atmosphere is an important process for many gases. Important examples include carbon dioxide (CO_2), for which the oceans account for 25% of

the sink for anthropogenic emissions (Le Quéré et al., 2016), and dimethylsulfide (DMS), which has an oceanic source and influences cloud properties with implications for the global energy balance (Quinn and Bates, 2011). The magnitude and direction of air/sea gas transfer is typically represented by Flux=$K\Delta C$ (Liss and Slater, 1974), where ΔC is the concentration difference across the air-sea interface and K is the gas transfer velocity. Direct flux measurements (Bell et al., 2013; Yang et al., 2013; Miller et al., 2010) are only possible for a small number of gases and are not made routinely. Most flux estimates use a wind speed-based parameterisation of K (e.g. Wanninkhof, 2014) coupled with measurements of ΔC.

CO_2 is the most well-observed trace gas in the surface ocean, with 14.5 million measurements compiled into a global database, the Surface Ocean CO_2 Atlas (SOCAT), http://www.socat.info/ (Bakker et al., 2016). Global trace gas databases also exist for gases such as methane and nitrous oxide https://memento.geomar.de/ (Bange et al., 2009), dimethylsulfide http://saga.pmel.noaa.gov/dms/ (Lana et al., 2011) and halocarbons https://halocat.geomar.de/ (Ziska et al., 2013). Accurate estimation of air/sea flux requires concentration measurements that are representative of the interfacial concentration difference. Surface seawater samples are often collected from the underway seawater intake of research vessels, typically at 5-7 m depth. A source of potential error in air/sea flux calculations arises from the assumption of vertical homogeneity within the mixed layer (Robertson and Watson, 1992). If vertical concentration gradients exist in the mixed layer, then underway seawater is not representative of the interfacial layer, which could create a global sampling bias (McNeil and Merlivat, 1996).

Vertical gradients in trace gas concentrations have been observed under conditions that are favourable for near surface stratification (Royer et al., 2016). At low wind speeds, high solar irradiance can suppress the depth of shear-induced mixing to create a near surface layer several degrees warmer than the water below (Ward et al., 2004; Fairall et al., 1996). Near surface stratification in the marine environment can also be induced by freshwater inputs such as rain (Turk et al., 2010) and riverine discharge. Changes in surface seawater temperature and salinity alter the solubility of dissolved gases and thus the amount available for air/sea exchange (Woolf et al., 2016). Dissolved gases isolated in the upper few metres of the ocean may additionally be modified by physical process such as air/sea exchange and photochemistry. Marine biota confined within the stratified layer (Durham et al., 2009), may

1   also alter trace gas concentrations. For the purposes of this paper, near surface gradients are

2   defined as physical and/or chemical gradients in the upper 10 m of the ocean.

3   Identifying and quantifying near surface gradients in trace gas concentrations is challenging.

4   Ship motion often inhibits near surface measurements made with the standard oceanographic

5   approach of sampling with Niskin bottles mounted on a CTD rosette. Substantial vertical

6   movement of the rosette limits how close to the surface a sample can be taken. For example, a

7   crane arm 4 m above the sea surface and 11 m from the centreline of a ship that is rolling by

8   ±4 degrees will induce ~1.5 m sample depth variation every few seconds. CTD/Niskin bottle

9   sampling requires that the rosette is kept below the sea surface. Sampling within 2 m of the

10   sea surface is often impossible, even under relatively calm conditions.

11   We present a Near Surface Ocean Profiling buoy (NSOP) designed for measuring near surface

12   profiles. The design principles for NSOP were:

13   (1) Platform diameter less than the wavelength of most open ocean waves, allowing it to ride

14   the swell;

15   (2) Short sampling arm close to the sea surface to reduce vertical movements induced by

16   platform motion;

17   (3) Capable of deployment close to the ship (to retrieve water for trace gas analysis), but away

18   from major turbulence and motion due to the ship itself.

19   Example profiles from a cruise on the European continental shelf (*RRS Discovery*, DY033,

20   July 2015) and in the English Channel on board the *RV Plymouth Quest* (part of the Western

21   Channel Observatory, Smyth et al., 2010, April 2014) are discussed.

23   **2   Methods**

24   **2.1   Near Surface Ocean Profiler (NSOP) description**

25   NSOP is a repurposed ocean buoy (1.6 m diameter) with a central lifting eyelet (Fig. 1). The

26   top of the buoy is 0.5 m above the sea surface. Mounted on top of the buoy are a line of sight,

27   remotely operated winch (Warrior Winch, model C8000) and a gel battery (Haze, model

28   HZY-S112-230). The winch feeds Kevlar rope through a block and tackle with a 3:1 ratio to

29   reduce rope pay-out speed to ~0.05 m s^{-1}. The block and tackle is attached to the end of an

1 outstretched arm 0.25 m from the outer edge of the buoy. The winch line is attached to an

2 open frame (0.35 m diameter, 0.8 m height) with the capacity to house multiple sensors.

3 Desired sampling depth is targeted using knowledge of the winch pay-out speed. Rope pay-

4 out is then timed with a stopwatch. This approach only approximately regulates the sampling

5 depth because: (i) winch pay-out varies slightly depending on the amount of rope on the

6 spool; and (ii) variable horizontal current strength affects the vertical versus horizontal

7 position of the sampling frame. To minimise horizontal movement of the sampling frame we

8 attached a 10 kg weight to the base of the frame.

9 The primary sensor on the sampling frame is a small CTD (Valeport miniCTD) set to sample

10 at a high frequency (>1 Hz). Under calm conditions it is possible to sample as close as 0.1 m

11 from the air/sea interface when the miniCTD and tubing are mounted near the top of the

12 frame. Rougher conditions demand that the frame be kept deeper (~0.5 m) as motion can

13 momentarily bring the sensors and tubing out of the water. An emergency tag line was

14 attached to the sampling frame in case the winch line failed. Seawater for trace gas analysis

15 was pumped back to the ship at 3.5 L min^{-1} through a 50 m PVC hose (0.5 in inner diameter).

16 A heavy duty peristaltic pump (Watson Marlow, model 701IB/R), primed with water from the

17 ships underway supply was used to overcome the large hydraulic head (~4 m). The open end

18 of the tubing was located at the same depth as the miniCTD. Water arriving to the ship's

19 laboratory was divided, with ~3.0 L min^{-1} for flow-through analysis (e.g. equilibrator for trace

20 gases) and ~0.5 L min^{-1} for discrete samples (e.g. total alkalinity).

21 We assessed the depth resolution capability of NSOP at a particular depth by looking at

22 pressure variations under calm conditions with a fixed amount of winch rope paid out. In calm

23 to moderate conditions (<2.5 m significant wave height) the amount of vertical movement

24 indicated by the standard deviation (SD) in the depth is ±0.18 m (Fig. S1, supplementary

25 information). During 4 deployments in rough conditions (>2.5 m significant wave height), the

26 depth variability increased as the sampling frame was lowered (at 5 m, SD was ±0.275 m).

27 **2.2 NSOP deployment**

28 On a large research vessel such as the *RRS Discovery*, the deployment and recovery of NSOP

29 requires close coordination between the bridge and 3 personnel on deck. NSOP was always

30 deployed while the ship was on station and not at the same time as other overboard

31 deployments. Ship orientation during deployments was typically with bow into the wind but

1   also accounted for swell and current direction/speed. NSOP was lifted by the aft crane (Fig.

2   1). Once NSOP was lowered to the surface it was detached from the crane via a quick release.

3   Two slack lines were looped through eyelets on the free-floating NSOP to maintain its

4   position close to the ship. A third slack line was connected to the top of the buoy and passed

5   through a block on a fully extended crane arm of 7 m to maintain this distance between NSOP

6   and the ship. The slack lines successfully inhibited the tendency of NSOP to drift horizontally

7   without disrupting its ability to ride the swell. The instrument frame acted like a sea anchor

8   and minimised rotation of NSOP. A 4 m lifting strop used for recovery was connected to the

9   lifting eyelet and loosely lashed to the aft slack line. During retrieval, the slack lines were

10   hauled in and the crane and jib arms brought towards the ship to bring NSOP alongside. The

11   lifting strop was then parted from the slack line and attached to the crane to lift NSOP back on

12   deck. For additional photographs of a NSOP deployment and videos of NSOP during a

13   deployment and in operation see Fig. S2 and videos, supplementary information.

14   Turbulence from the ship's propellers has the potential to mix the water column and destroy

15   any near surface gradients. The ship did not use the aft thrusters whenever conditions were

16   suitable (mild sea state, weak currents and no local hazards). Keeping NSOP away from the

17   ship limited disruption of near surface gradients by the thrusters and reduced the risk of line

18   entanglement in the aft propellers. Our winch did not have a groove bar to feed the rope onto

19   the winch drum, leading to an increased likelihood of snagging during spooling. To minimize

20   snagging, the rope was manually fed onto the winch spool before deployments. Visual

21   monitoring of the NSOP frame, slack lines and winch spool is important during deployment.

22   NSOP has been successfully deployed in 'moderate' sea states up to Beaufort force 5 (~10 m

23   s^{-1} wind speed and wave heights of ~2.0 m). Deployment length typically varied from 1-3

24   hours.

25
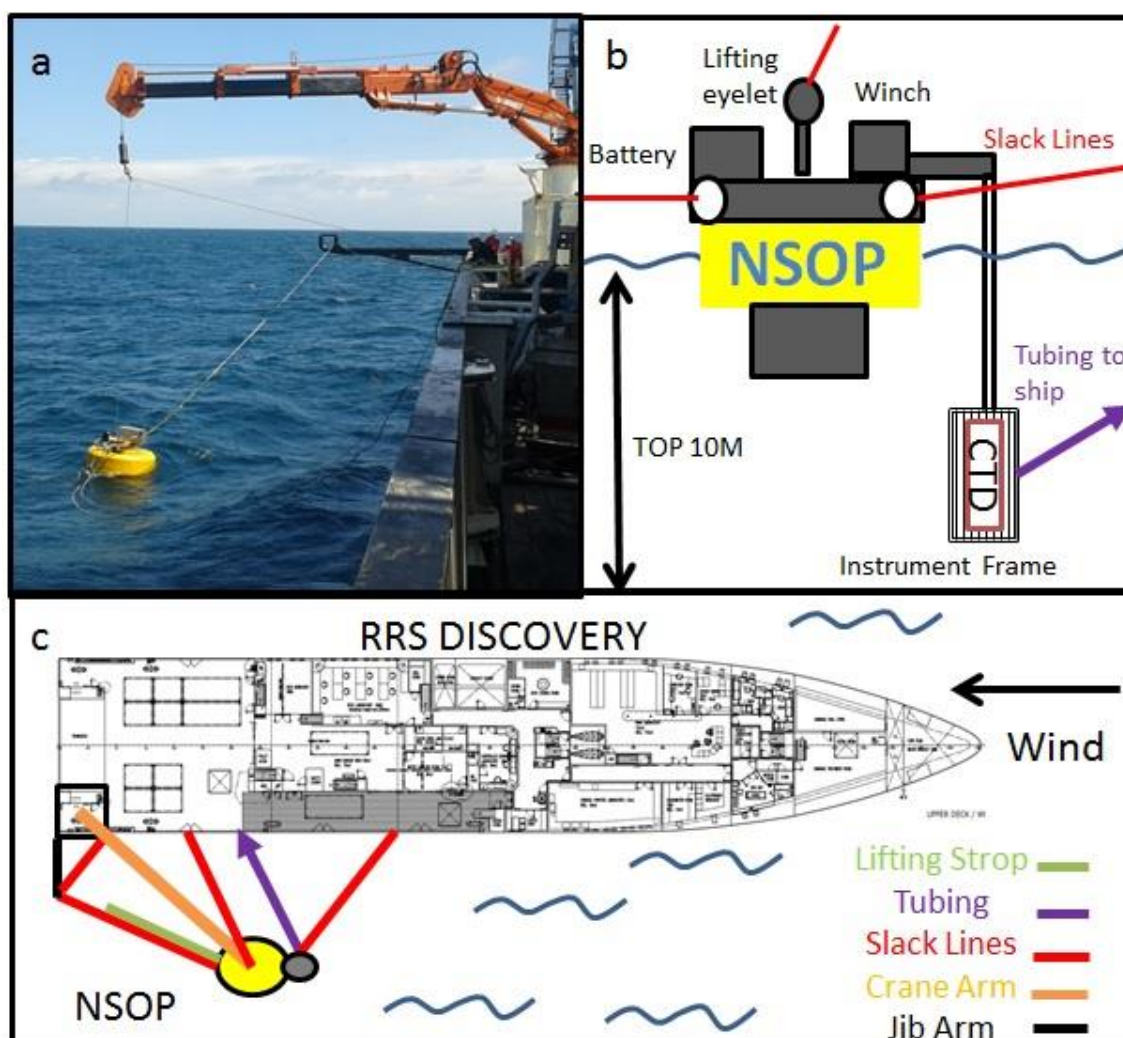
2 **Figure 1:** Different points of view of an NSOP deployment: (a) Image from a deployment on
3 *RRS Discovery* in May 2015 (Cruise DY030); (b) Schematic cross section of NSOP including
4 tubing back to ship (purple) and slack lines (red); and (c) Top down schematic from a research
5 ship including ship orientation. Not to scale.

7 NSOP can be used in two profiling modes: 'continuous' and 'discrete'. Continuous profiling

8 maximises vertical coverage and involves the winch continuously paying rope in and out at

9 ~0.05 m s^{-1}. A complete down/up profile to 10 m can be conducted in approximately 7

10 minDepth resolution during continuous profiling is determined by the measurement response

11 time. Instruments with rapid response times such as the miniCTD temperature and

12 conductivity sensors (0.15 s and 0.09 s) have theoretical depth resolutions of 0.75 cm and

13 0.45 cm respectively. Actual depth resolution will also be affected by the sampling depth

14 variability of the NSOP instrument frame. A measurement setup with a longer response time

15 (such as for seawater CO_2) requires a different approach (see Section 2.5).

1   During discrete profiling, the winch pays out a fixed amount of rope (typically 0.5 m) and the

2   sampling frame is left at a fixed depth. After a fixed sampling period, more rope is paid out.

3   The process is repeated down and then up such that a set of discrete depths are sampled in a

4   'stepped' profile. The discrete profiling depth resolution is determined by the depth

5   fluctuations when sampling at a fixed depth (see Section 2.1). Discrete profiles are a more

6   appropriate approach for measurement systems with a longer response time. A discrete profile

7   with 0.5 m steps down to 5 m and back to the surface using a 2.5 min sampling period takes

8   about an hour. The sampling period at each depth and frequency/distribution of depths within

9   the profile can be adjusted to suit sampling priorities.

10   The maximum deployment time is limited by the capacity of the winch battery. When under

11   no load, the battery allows for approximately 3 hours of operation in the continuous mode.

12   Discrete profiling requires substantially less winch usage such that battery drainage is even

13   less of a concern.

14   **2.3 CO_2 analysis**

15   The CO_2 measurement system (Fig. 2) is a modified version of the system described by

16   (Hales et al., 2004). Seawater from the NSOP inlet was passed through the equilibrator (see

17   Section 2.3.1) at ~3 L min^{-1} and the flow rate monitored (Cynergy ultrasonic flow meter,

18   model UF25B). A compressed nitrogen gas supply, maintained at a constant flow rate of 100

19   mL min^{-1} (Bronkhurst mass flow controller, model F-201-CV-100) flows through the

20   equilibrator in the opposite direction to the seawater flow. The gas has high water vapour

21   content after equilibration and is dried (Permapure nafion dryer, model MD-110-48S-4). The

22   dried sample then enters the analytical cell of a NDIR Licor 7000, which is protected with a

23   0.2 µm filter (Pall, Acro 50).

24   CO_2 measurements at atmospheric pressure as recommended by Dickson et al. (2007) were

25   not possible due to the nature of the experimental setup. The continuous gas flow through the

26   system caused a small 0.4 kPa pressure increase in the Licor measurement cell, this was in

27   good agreement with a similar observation by Burke Hales (0.5kpa > ambient pressure;

28   Personal communication). The elevated pressure was taken to be representative of the

29   equilibrator pressure and was used to obtain the partial pressure of CO_2 in the equilibrator

30   ($pCO_{2(eq)}$).

1   The Licor was calibrated using three CO_2 standard gases before and after each NSOP

2   deployment. The concentrations of the standard gases (BOC Ltd.) were determined by

3   referencing against US National Oceanic and Atmospheric Administration certified standards

4   (244.91, 388.62, 444.40 ppm) in the laboratory. The seawater temperature at the entry and

5   exit ports of the equilibrator was recorded at 1 Hz (Omega ultra-precise 1/10 DIN immersion

6   RTD) using stackable microcontrollers (Tinkerforge master brick 2.1 and PTC bricklet).

7   Equilibrator temperature probes and the miniCTD temperature sensor were calibrated before

8   and after each cruise against an accurate reference sensor (Fluke, model 5616-12, ±0.011°C)

9   in a stable water bath (Fluke 7321).
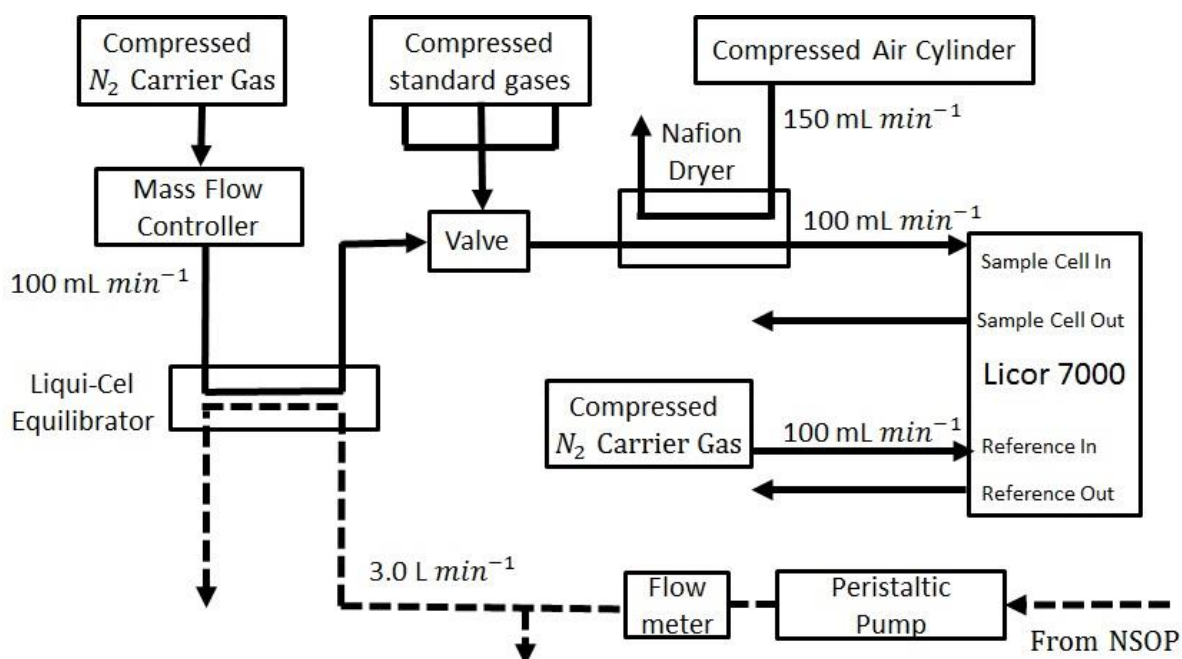
12 **Figure 2:** CO_2 system schematic. Solid and dashed arrows correspond to gas and water flows
13 respectively. The Licor reference cell is flushed with equilibrated gas at 100 mL min^{-1}. A
14 manual selection valve was used to switch between equilibrated gas and the CO_2 standards.

16   2.3.1   Equilibrator

17   The showerhead equilibrator is the most commonly-used equilibrator for CO_2 but takes ~100

18   s to equilibrate (Dickson et al., 2007; Kitidis et al., 2012; Körtzinger et al., 2000; Webb et al.,

19   2016). This equilibration time is too slow for effective use during NSOP deployments. We

20   used a polypropylene membrane equilibrator (Liqui-Cel, model 2.5x8) with liquid and gas

1   volumes of 0.4 L and 0.15 L and a surface are aof 1.4 m^2. Due to its large surface area to

2   volume ratio and membrane porosity (50%), the Liqui-Cel expedites gas transfer and

3   efficiently achieves equilibration (Loose et al., 2009), with a 3 s response time for CO_2 (Hales

4   et al., 2004). Membrane equilibrators have been used by others for trace gas analysis (Hales et

5   al., 2004; Marandino et al., 2009).

6   Fugacity of seawater CO_2 is calculated from the Licor gas phase CO_2 measurement. This

7   approach assumes that the gas phase sample has equilibrated fully with the seawater. We

8   performed equilibration efficiency experiments in a seawater tank using a showerhead

9   equilibrator as a reference. Liqui-Cel equilibration efficency declined after prolonged

10   exposure to seawater, likely due to biofouling of the membranes. In a fouled equilibrator,

11   equilibration efficency was a function of the flow rate on both the water and gas side of the

12   membrane. An increased gas flow rate reduces the residence time inside the Liqui-Cel and

13   allows less time to equilibrate (Fig. 3a). Increasing the waterside flow rate moves the gas

14   phase closer to equilibrium because the transfer coefficent in the membrane increases (Fig.

15   3b).

16   Cleaning with an acid - base sequence restored the efficiency of a fouled equilibrator. It was

17   necessary to actively pump chemicals through the Liqui-Cel to achieve a full recovery in

18   efficiency. For more details on cleaning techniques, see supplemental material. Efficiency

19   reductions in membrane equilibrators like the Liqui-Cel have not been reported by previous

20   studies. Some authors have used 5-50 μm filters to minimise biofouling (Hales et al., 2004)

21   but this was not possible with the NSOP experimental design. If filtering seawater is not

22   possible, we recommend flushing with freshwater after use, regular cleaning of the Liqui-Cel

23   and daily tests to quantify equilibration efficiency. Trace gas measurement systems that use

24   an internal liquid phase standard (e.g. dimethylsulfide, Section 2.4) account for any changes

25   in equilibrator efficiency.

26

27
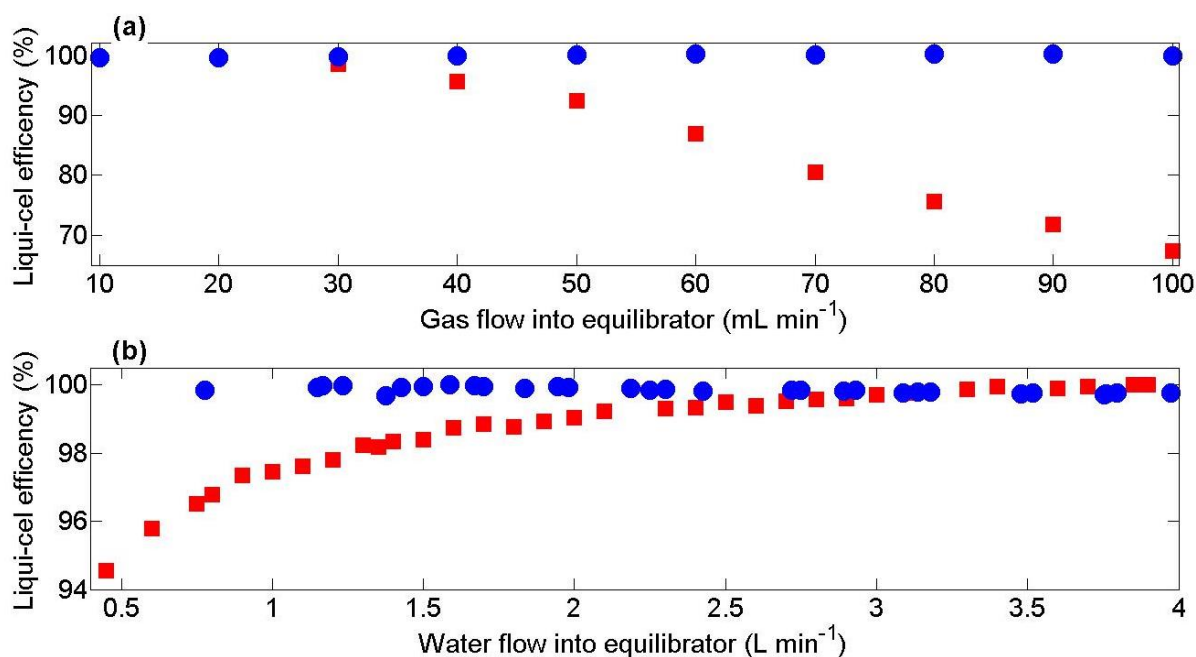
1 **Figure 3:** Liqui-Cel CO_2 equilibration efficiency (Liqui-Cel mixing ratio / showerhead
2 mixing ratio) for: (a) changing gas flow at a fixed water flow rate of 4 L min⁻¹; and (b)
3 changing water flow at a fixed gas flow of 100 mL min⁻¹. Blue = unfouled equilibrator. Red =
4 fouled equilibrator.

6 **2.4   DMS analysis**

7 DMS was measured with Atmospheric Pressure-Chemical Ionisation Mass Spectrometry

8 (API-CIMS), using a system modified following Saltzman et al. (2009). Measurements were

9 calibrated using an isotopic liquid standard of tri-deuterated DMS (see Bell et al., 2013 for

10 details). Isotopic standard was injected at 120 μL min⁻¹ into the 3 L min⁻¹ seawater flow from

11 NSOP before it entered the Liqui-Cel equilibrator. Compressed nitrogen gas was passed

12 through the equilibrator in the counter direction to the seawater flow at 1 L min⁻¹. The use of

13 an internal standard meant that any incomplete equilibration of the ambient non-isotopic DMS

14 was also true for the isotope. The gas stream exited the equilibrator and was dried (Permapure

15 nafion dryer, model MD-110-48S-4) before entering the mass spectrometer for analysis. DMS

16 was detected at m/z (mass/charge) 63 and the isotopic standard detected at m/z 66. The

17 concentration of DMS was calculated using the ion signals and relevant flow rates (Bell et al.,

18 2015). This approach has been shown to compare well with other analytical techniques for

19 DMS (Royer et al., 2014; Walker et al., 2016).

2.5   NSOP delay and response time

We used different approaches to assess the delay between instantaneous miniCTD measurements and water arriving to the ship for analysis. The delay between seawater entering the inlet and reaching the equilibrator was calculated as 114 s using the internal volume of NSOP tubing (0.5 in inner diameter, 54 m length) and a seawater flow rate of 4.15 L min^{-1}. Delay correlation analysis between the NSOP miniCTD temperature sensor and a second sensor positioned at the entrance to the equilibrator gives a similar delay of 112 s. Note that the total delay of the system is greater because it also includes the time that equilibrated gas takes to reach the Licor. We determined the total delay by quickly transferring the seawater inlet quickly between two buckets with distinctly different CO_2 concentrations and timing how long it took for the signal to be detected by the Licor (139 s; Fig. 4).

The response time of the NSOP setup was determined by simulating step changes in gas concentrations. A model fit to the exponential change in signal was used to estimate the response time (Fig. 4). We estimate the system response time (e-folding time) for CO_2 as 24 s, which is slightly faster than the 34 s reported by Webb et al. (2016). The e-folding time in the DMS signal is estimated as 11 s, which is consistent with the rapid gas flow rate through the analytical system.

Continuous profiling with the CO_2 system and a 24 s response time yields a depth resolution of 1.2 m, which is greater than the required resolution to assess near surface gradients. DMS has a faster response time than CO_2, but in continuous profiling mode this only translates to a depth resolution of 0.6 m, slightly less than the 1.2-2 m reported by (Royer et al., 2014). A depth resolution of < 0.5 m was desired to capture upper ocean vertical gradients in CO_2 and DMS so NSOP was operated in discrete profiling mode.
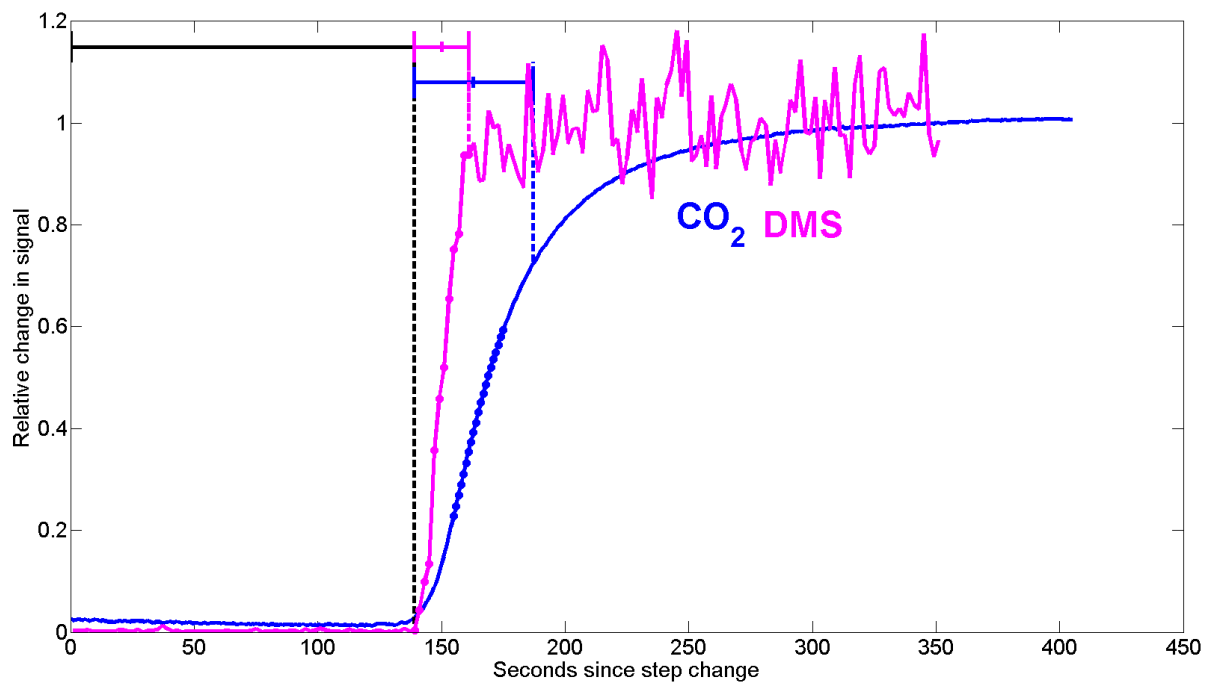
2 **Figure 4:** Instrument responses to step changes in seawater CO_2 (blue) and DMS (magenta).
3 Instrument responses have been scaled so that the initial and end concentrations are between 0
4 and 1. Time is referenced against the point when the step change was initiated. The response
5 is seen in both instruments after a delay of 138 s (black dashed line). Two e-foldings are
6 indicated by vertical dashed lines for CO_2 (blue) and DMS (magenta). The data points marked
7 by circles were used to make an exponential fit to the data to determine the response time
8 (Sect 2.5).

11 **2.6   Data processing**

12 During discrete profiling, distinct sample depths were identified from the rapid changes in

13 pressure during depth transitions. Data were binned into discrete depth bins using CTD

14 pressure measurements. Trace gas data were assigned to depth bins after adjusting for the

15 calculated transit time through the NSOP tubing (Section 2.5). CO_2 data from the beginning

16 (2 e-foldings + 15 s buffer = 63 s) and end (15 s buffer) of each depth bin was excluded from

17 analysis to account for the response time of the system and the transition time between sample

18 depths. The same approach was taken for DMS, where the faster response time resulted in a

19 smaller portion of data excluded at the beginning of each depth bin (2 e-foldings + 15 s buffer

20 = 37 s).

1 The CO_2 mixing ratio (xCO_2) measured in the Licor is converted to equilibrator fugacity

2 ($fCO_{2(eq)}$) using calibration standards, *in situ* seawater salinity, and the pressure and

3 temperature in the equilibrator (SOP 5# Underway pCO2 Dickson et al., 2007). Vertical

4 profiles of seawater CO_2 fugacity ($fCO_{2(sw)}$) are calculated using average equilibrator fugacity

5 ($fCO_{2(eq)}$), equilibrator temperature ($T_{(eq)}$) and *in situ* seawater temperature ($T_{(sw)}$) at each

6 depth (Takahashi et al., 1993).

7 **2.7   Seawater sample collection using NSOP**

8 The NSOP setup enables vertical profiles of discrete seawater samples to be collected from

9 upstream of the equilibrator, with a split in the tubing diverting ~0.5 L min^{-1} into a sink. For

10 example, discrete seawater samples (250 ml) have been successfully collected and analysed

11 for Total Alkalinity (TA). Samples were collected and poisoned following best practice

12 recommendations (SOP#1, (Dickson et al., 2007). Bottle filling plus 1 overfill took ~60 s.

13 Start and end times were recorded so that collection depth could be retrospectively

14 determined from the CTD pressure data. Analytical methods and an example depth profile are

15 provided in the supplementary information.

17 **3   Field Measurements / Observations**

18 Presented below are example profiles collected using NSOP. The first deployment was in the

19 open ocean (July 30th 2015, Central Celtic Sea; 49.4213°N, -8.5783°E) from the *RRS*

20 *Discovery* (100 m length, 6.5 m draught). The second deployment was in coastal waters (15th

21 April 2014, Plymouth Sound; 50.348°N, -4.126°E) from the *RV Plymouth Quest* (20 m

22 length, 3 m draught). A map of deployment sites is supplied in the supplementary

23 information.

24 **3.1   Open ocean deployment**

25 NSOP was deployed at 14:05 (UTC) on 30th July 2015. During the 6 hours preceding

26 deployment, the ship was on station and encountered persistently strong solar radiance (> 600

27 W m^{-2}), mild winds (< 6 m s^{-1}) and calm sea state (significant wave height < 1.6 m). This

28 combination of low wind speeds and high irradiance (Fig. S5, supplementary information) is

29 favourable for near surface stratification (Donlon et al., 2002).

2 Fig. 5 presents the time series data collected by NSOP for depth, temperature, salinity and

3 $fCO_{2(sw)}$. Discrete profiling began at 14:05 hrs (UTC) at 0.7 m depth, which was as close to

4 the surface as the frame could be located without the possibility of breaking the surface.

5 Depth bins were identified based on rapid depth transitions (Fig. 5a). Bottles were filled for

6 discrete samples during the downcast. Profiling lasted 75 minutes and finished back at the

7 surface at 15:20 hrs (UTC). Seawater temperature was 16.61 ± 0.06 °C. At 14:20 hrs (UTC)

8 $fCO_{2(atm)}$ was 398 µatm and$fCO_{2(sw)}$ was 389 µatm at 0.67 m meaning the ocean was

9 undersaturated with respect to the atmosphere. The temperature and seawater CO_2 were the

10 expected magnitude for summer in the Celtic Sea (Frankignoulle and Borges, 2001). Salinity

11 was homogeneous throughout the NSOP deployment, only varying by ±0.004.
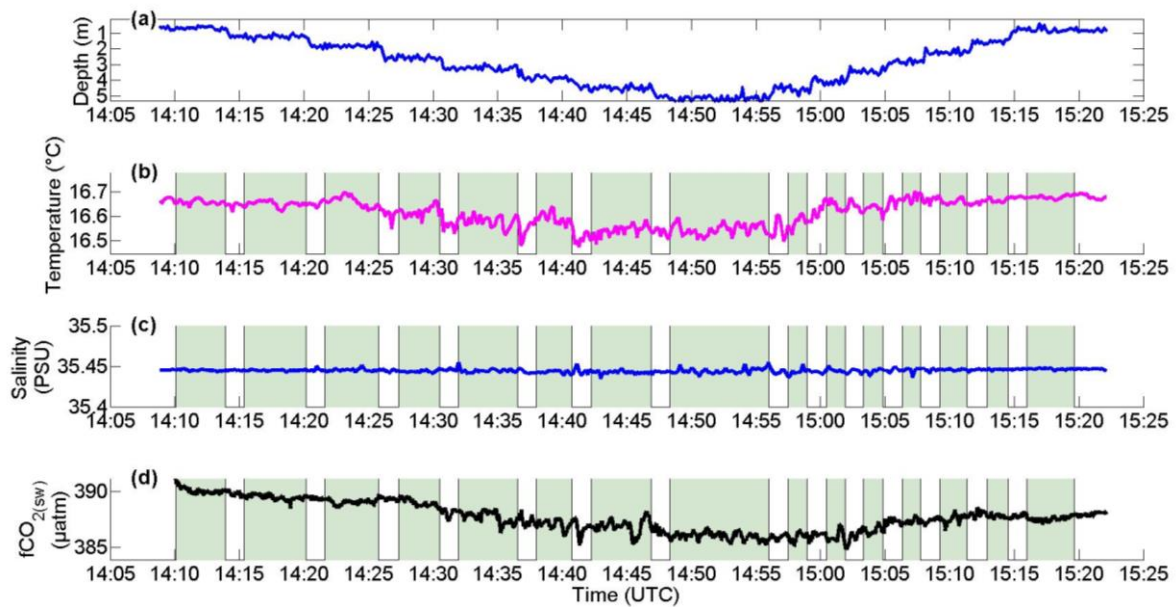
13 **Figure 5:** Time series measurements made during an NSOP deployment in the Celtic Sea on
14 30th July 2015. Data are 1 Hz depth (a), seawater temperature (b), salinity (c) and $fCO_{2(sw)}$ (d).
15 Data used for depth bin analysis (Section 2.6) is identified by a shaded background.

17 Depth-binned salinity and temperature data did not show any significant variability (Fig. 6a).

18 A slight temperature gradient was observed, with 0.15°C difference between 5 m and the

19 surface and a fairly constant reduction with depth (0.03°C per metre). The temperature profile

20 was similar for down and up casts, although some continued warming of surface waters was

21 evident in the up cast. The temperature measured by NSOP at 5.15 m depth agrees well with

22 the coincident temperature measured by the bow thermistor at 5.5 m (< 0.02°C difference)

1 (Fig. 6c). There is no evidence that the ship's thrusters/propellers disrupted the near surface

2 gradients.

3 We compare the NSOP temperature profile with thermistor readings from a series of Sea-Bird

4 Scientific (SBE 56) sensors (0.3, 0.6, 1.5, 3.5 and 7 m depth) mounted on a nearby

5 temperature chain moored ~2.8 km away (49.403°N, -8.606°E) from the deployment site .

6 The vertical profile implied by the NSOP deployment agrees with the mooring data (Fig. 6c),

7 and corroborates the warming of the upper few metres of the ocean observed during the

8 deployment. The agreement between these independent datasets suggests that it is unlikely

9 that NSOP caused any significant localized warming of surface waters. The mean difference

10 between NSOP temperature from discrete depths and the mooring sensors is 0.02°C. The

11 surface data from the NSOP up cast show less agreement with the mooring, with NSOP

12 temperatures ~0.05 °C lower than the 0.3 m and 0.6 m mooring sensors. During the profile the

13 ship drifted ~1 km from the start position of the profile and a further 0.2 km from the

14 mooring. The small offset between the NSOP surface temperatures and the mooring may be

15 driven by horizontal variability between the deployment and mooring locations. It is also

16 possible that turbulence mixed warm surface waters down into cooler sub-surface layers.

17 Turbulence could have been generated around the NSOP sampling frame or by an increase in

18 wave-driven mixing when the significant wave height increased at ~15:00 hrs UTC (Fig.

19 S4a).
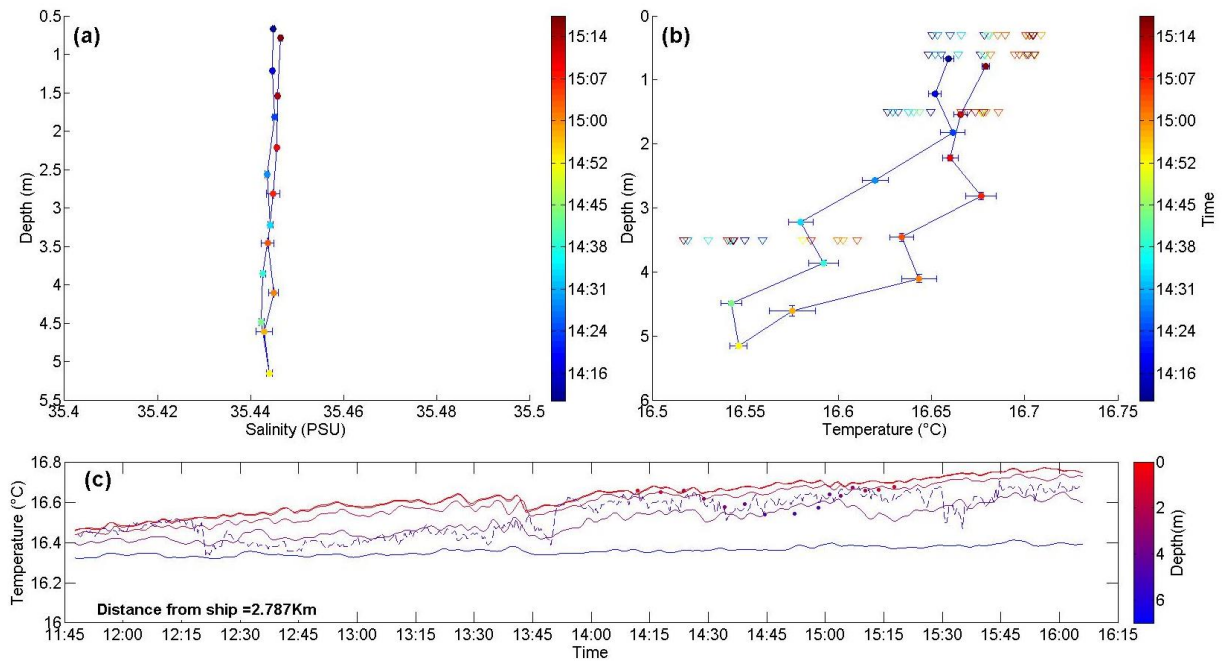
Figure 6: Salinity and temperature in the Central Celtic Sea on 30th July 2015. NSOP profiles of salinity (a) and temperature (b) were derived using depth bins as described in Section 2.6. Data points are coloured by sampling time. Vertical and horizontal error bars show two standard errors of the mean in each depth bin. Coloured triangles in (B) are time-averaged temperature for four depths (0.3, 0.6, 1.5 and 3.5 m) at the nearby Central Celtic Sea temperature mooring (49.403°N, -8.606°E). (c) Timeseries of temperature at the mooring. Timeseries of temperature at depths (0.3, 0.6, 1.5 and 3.5 m) are solid lines whereas the dashed line is the underway temperature at 5.5 m from *RRS Discovery* (located 2.8 km from the mooring). The mooring and underway temperatures are coloured according to their sample depth, where red is the air/sea interface. The circles are binned temperature data from NSOP which have also been coloured to reflect the depth of collection.

Seawater density (Fig. 7a) was calculated using the salinity and temperature profile data (Fig. 6a &6b) and the 1983 Unesco equation of state (Millero and Poisson, 1981). As expected with little variation in the salinity, changes in the density profile are dominated by temperature. The down and up casts for CO_2 show excellent agreement below 2.5 m. Surface water (< 2 m) CO_2 is 2-4 μatm higher than at 5 m (Fig. 7b). Elevated surface CO_2 could be explained by a sustained flux from the atmosphere into a near surface stratified layer with inhibited deep water exchange. Under this assumption a vertical gradient in seawater CO_2 would need to be established shortly after the temperature gradient. A paired t-test showed that the fCO_2 measured in the surface bins on the downcast and upcast are were significantly different ($p = <0.001$) . The deepening of the surface stratified layer could explain the more homogeneous CO_2 during the upcast. It is worth noting that in addition to physical processes, plankton trapped within the surface layer could also modify the surface CO_2. Trace gas concentrations may also be different in the sea surface microlayer but sampling that close to the surface is beyond the capabilities of NSOP. Complimentary measurements of the sea surface microlayer could be made using other state of the art purpose built sampling platforms such as the Sea Surface Scanner (Ribas-Ribas et al., 2017).
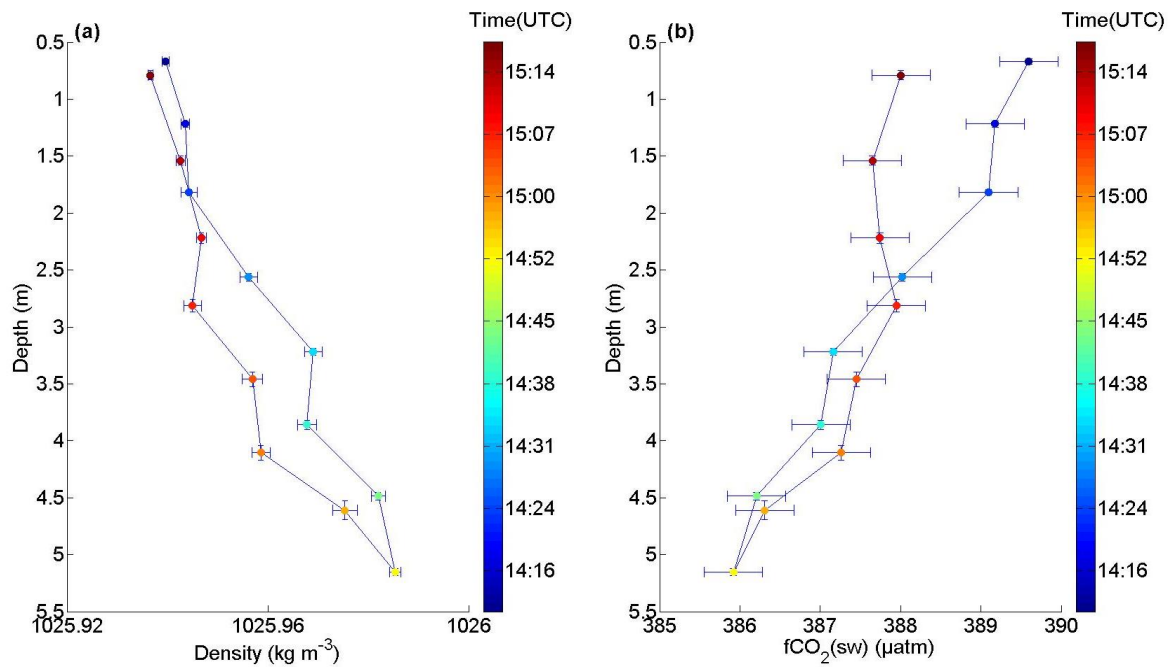
Figure 7: NSOP density (a) and $fCO_{2(sw)}$ (b) profiles from the Celtic Sea on 30th July 2015. Data points are coloured by sample time. Vertical error bars correspond to two standard errors of the mean in each depth bin. The horizontal error bars in (a) are two standard errors of the mean, whereas in (b) they are the propogated error from the the binned measurements used to calculate $fCO_{2(sw)}$.

To assess measurement accuracy the NSOP Liqui-Cel CO_2 system was compared against an independent CO_2 system that had a showerhead equilibrator coupled to the ship's seawater supply pumped from 5.5 m below the sea surface (Hardman-Mountford et al., 2008; Kitidis et al., 2012). Technical issues meant that the underway CO_2 system installed on the *RRS Discovery* was not functioning during the deployment detailed above. However during a deployment on the 19th July 2015, the $fCO_{2(sw)}$ measured by NSOP at 5 m agreed well with independent measurements from the underway system, difference = 1.7+/- 4.18 µatm. The agreement between the two systems is in line with previous intercomparisons (Ribas-Ribas et al., 2014; Körtzinger et al., 2000).

3.2   Coastal deployment

DMS profiles were collected on a small research vessel on 15th April 2014. NSOP was deployed within the Plymouth Sound at 12:00 hrs UTC and recovered 95 minutes later (Fig. 8). In the sheltered environment behind the breakwater the standard deviation in depth was

1 ±0.10 m, smaller than observed during open ocean profiles. Seawater temperature and salinity

2 demonstrate clear structure, with lower temperatures and higher salinities associated with sub-

3 surface water. Two river estuaries (Plym and Tamar) converge and flow out to the open ocean

4 through the Plymouth Sound. We likely observed a freshwater surface lens that was protected

5 from wave-driven mixing and had been warmed over the course of the day. We used a

6 different miniCTD during this deployment and were thus also able to collect fluorescence

7 data (Fig. 8d).

8 Temperature profiles (Fig. 9a) show a sharp discontinuity in the downcast at ~5 m whereas in

9 the upcast the thermocline had shoaled to ~3.5 m. The salinity profiles suggest similar mixing

10 depths to the temperature profiles, with lower salinity water at the surface (Fig. 9b).

11 Fluorescence increases with depth (Fig. 9c), but this is likely due to quenching of the

12 phytoplankton photosynthetic apparatus at the surface(Smyth et al., 2004). DMS

13 concentrations reduce steadily with depth (Fig. 9d), which is likely explained by changes in

14 DMS production and consumption rates by the biological community (Galí et al., 2013). The

15 DMS profiles from the upcast and the downcast are very similar, with the largest difference at

16 the very surface. A large difference in the surface-most data point can also be seen in the

17 temperature data, and may reflect mixing with sub-surface waters due to the motion of NSOP

18 or short time-scale variations in the physical environment.
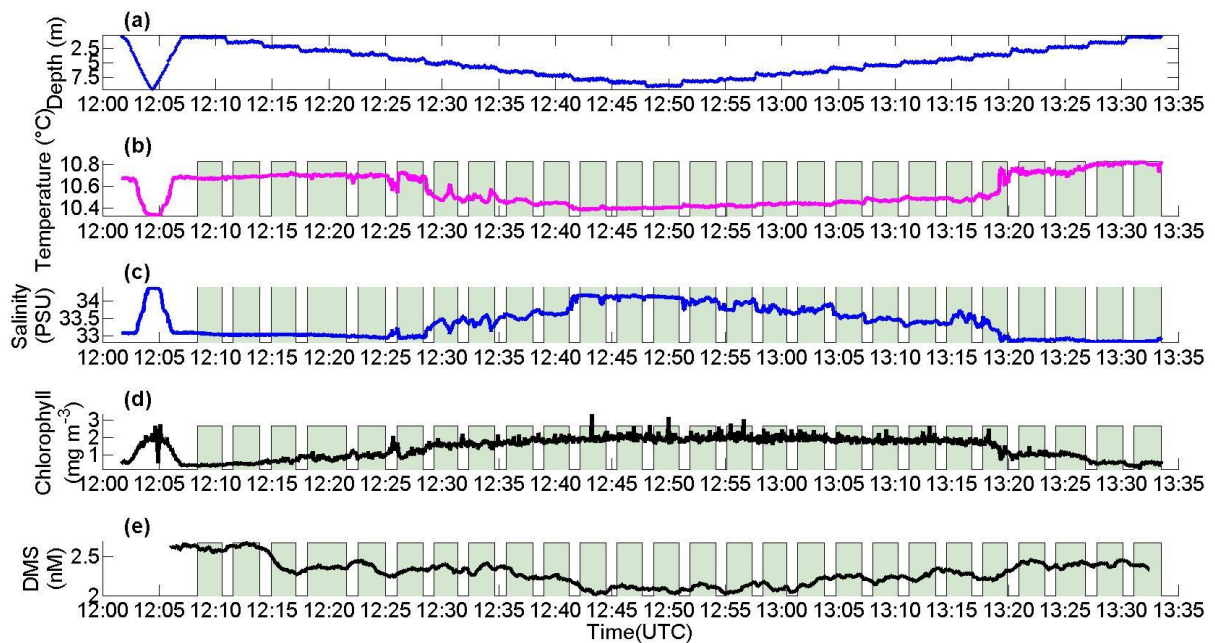
20 **Figure 8:** Time series measurements during an NSOP deployment in Plymouth Sound on 15th
21 April 2014: depth (a), temperature (b), salinity (c), chlorophyll fluorescence (d) and DMS(sw)

 (e). Data used for depth bin analysis (Section 2.6) is identified by a shaded background. The
beginning of the time series is an example off a continuous profile (see Section 2.2).
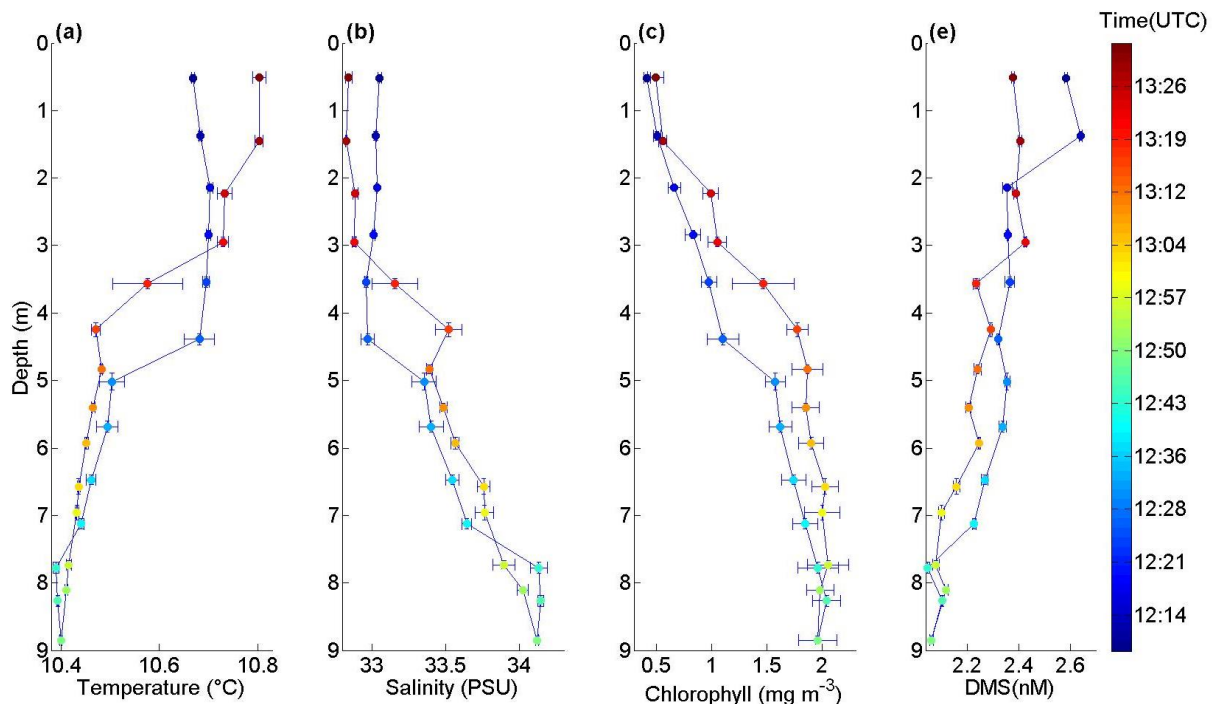
Figure 9: NSOP profiles collected in Plymouth Sound on 15th April 2014: temperature (a),
salinity (b), chlorophyll fluorescence (c), and DMS$_{(sw)}$ (d). Data are coloured by sample time.
Vertical and horizontal error bars are two standard errors of the mean (SEM) in each depth
bin.

4   Summary

This paper describes a Near Surface Ocean Profiler (NSOP) designed to measure vertical

trace gas profiles near the air-sea interface. NSOP is unique in approach as its sampling frame

is lowered from a buoy that rides the ocean swell, reducing relative motion of the frame and

hence fluctuations in sampling depth. The NSOP design facilitates near surface (< 0.5 m)

sampling, significantly improving the capability to resolve vertical gradients. Other benefits

include the ability to sample away from ship-driven turbulence and the flexibility to make a

large range of near surface measurements. The NSOP sampling frame houses the miniCTD

and also has the capacity to incorporate additional sensors (e.g. turbulence, dissolved oxygen

and other measures of phytoplankton abundance and photosynthetic health). The ability to

collect water from discrete depths facilitates the collection of near surface samples that

require additional processing or take longer to analyse (e.g. TA, dissolved inorganic carbon,

1   nutrients, the DMS-precursor DMSP, dissolved organic carbon). NSOP is highly versatile and

2   can be used for continuous or discrete profiling. Further development could adjust winch pay

3   out speed and enable continuous, high resolution depth profiles for slower response time

4   measurements (e.g. $fCO_{2(sw)}$).

5   Near surface stratification in the upper few metres of the ocean due to temperature and

6   salinity gradients is a well-documented phenomenon. The presence or absence of chemical

7   and biological gradients within near surface stratified layers has been difficult to assess.

8   NSOP is a platform with the capability to successfully resolve gradients in these near surface

9   layers. The data presented in this paper demonstrate that near surface gradients in trace gases

10   can lead to substantially different fluxes depending upon the seawater depth that is used to

11   calculate the flux. Assuming that the effect of temperature and salinity gradients on the flux

12   can be accounted for using remote sensing methods (e.g Shutler et al., 2016), then the change

13   in flux is directly proportional to the change in ΔC. In the case of the coastal DMS profile, a

14   higher concentration (2.58±0.02 nM) was observed 0.5 m below the sea surface compared to

15   concentrations at 5 m (2.36±0.03 nM). Assuming that the atmospheric concentration of DMS

16   was negligible (a typical approach for DMS fluxes, (see Lana et al., 2011) , computing the

17   flux with the 5 m waterside concentration instead of the 0. 5m waterside concentration means

18   the flux is underestimated by 9.3%. . In the case of the Celtic Sea CO_2 profile, the

19   concentration at 0.5 m (389.60 ±0.36 µatm) was higher than at 5 m (385.92 ±0.36 µatm). The

20   atmospheric CO_2 concentration was 398.1 ±0.3 µatm, which means that the surface water was

21   less undersaturated than implied by the seawater concentration at 5 m. Using the 5 m

22   waterside CO_2 concentration leads to an overestimation of the ΔC and flux by 43.5%

23   compared to using the 0.5 m waterside CO_2 concentration. The magnitudes of these

24   concentration gradients are significant. However, such gradients (in magnitude and direction)

25   do not persist for all hours of the day, under different environmental conditions and in all

26   regions of the global ocean. A subsequent publication will discuss NSOP data collected

27   during four cruises as well as the wider prevalence and implications of near surface CO_2

28   gradients

29   **Acknowledgements**

30   We thank the captains and crews of the *RV Plymouth Quest* and *RRS Discovery* for their

31   assistance with deploying NSOP, Christopher Balfour and Dave Sivyer for maintenance of

32   the Central Celtic Sea mooring near surface temperature sensors, Vassilis Kitidis for

1 supplying underway CO_2 data and Burke Hales for advice concerning Liqui-Cel CO_2

2 measurements. This research was made possible by PML internal funding, a NERC funded

3 studentship (NE/L000075/1), temperature sensors on the Central Celtic Sea mooring

4 (NE/K002058/1) and by the NERC Shelf Sea Biogeochemistry pelagic research programme

5 (NE/K002007/1). The *RRS Discovery* underway data was supplied by the Natural

6 Environment Research Council.

References

9 Bakker, D. C., Pfeil, B., Landa, C. S., Metzl, N., O'brien, K. M., Olsen, A., Smith, K., Cosca,
10 C., Harasawa, S., and Jones, S. D.: A multi-decade record of high-quality fCO 2 data in
11 version 3 of the Surface Ocean CO 2 Atlas (SOCAT), Earth System Science Data, 8, 383,
12 2016.

13 Bange, H. W., Bell, T. G., Cornejo, M., Freing, A., Uher, G., Upstill-Goddard, R. C., and
14 Zhang, G.: MEMENTO: a proposal to develop a database of marine nitrous oxide and
15 methane measurements, Environmental Chemistry, 6, 195-197, 2009.

16 Bell, T., De Bruyn, W., Miller, S., Ward, B., Christensen, K., and Saltzman, E.: Air–sea
17 dimethylsulfide (DMS) gas transfer in the North Atlantic: evidence for limited interfacial gas
18 exchange at high wind speed, Atmospheric Chemistry and Physics, 13, 11073-11087, 2013.

19 Bell, T., De Bruyn, W., Marandino, C. A., Miller, S., Law, C., Smith, M., and Saltzman, E.:
20 Dimethylsulfide gas transfer coefficients from algal blooms in the Southern Ocean,
21 Atmospheric Chemistry and Physics, 15, 1783-1794, 2015.

22 Dickson, A. G., Sabine, C. L., and Christian, J. R.: Guide to best practices for ocean CO_2
23 measurements, 2007.

24 Donlon, C., Minnett, P., Gentemann, C., Nightingale, T., Barton, I., Ward, B., and Murray,
25 M.: Toward improved validation of satellite sea surface skin temperature measurements for
26 climate research, Journal of Climate, 15, 353-369, 2002.

27 Durham, W. M., Kessler, J. O., and Stocker, R.: Disruption of vertical motility by shear
28 triggers formation of thin phytoplankton layers, Science, 323, 1067-1070, 2009.

29 Fairall, C., Bradley, E. F., Godfrey, J., Wick, G., Edson, J. B., and Young, G.: Cool-skin and
30 warm-layer effects on sea surface temperature, Journal of Geophysical Research, 101, 1295-
31 1308, 1996.

32 Frankignoulle, M., and Borges, A. V.: European continental shelf as a significant sink for
33 atmospheric carbon dioxide, Global Biogeochemical Cycles, 15, 569-576, 2001.

34 Galí, M., Simó, R., Vila-Costa, M., Ruiz-González, C., Gasol, J. M., and Matrai, P.: Diel
35 patterns of oceanic dimethylsulfide (DMS) cycling: Microbial and physical drivers, Global
36 Biogeochemical Cycles, 27, 620-636, 2013.

37 Hales, B., Chipman, D., and Takahashi, T.: High-frequency measurement of partial pressure
38 and total concentration of carbon dioxide in seawater using microporous hydrophobic
39 membrane contractors, Limnol. Oceanogr.: Methods 2, 356-364, 2004.

Hardman-Mountford, N. J., Moore, G., Bakker, D. C., Watson, A. J., Schuster, U., Barciela, R., Hines, A., Moncoiffé, G., Brown, J., and Dye, S.: An operational monitoring system to provide indicators of CO_2-related variables in the ocean, ICES Journal of Marine Science: Journal du Conseil, 65, 1498-1503, 2008.

Kitidis, V., Hardman-Mountford, N. J., Litt, E., Brown, I., Cummings, D., Hartman, S., Hydes, D., Fishwick, J. R., Harris, C., and Martinez-Vicente, V.: Seasonal dynamics of the carbonate system in the Western English Channel, Continental Shelf Research, 42, 30-40, 2012.

Körtzinger, A., Mintrop, L., Wallace, D. W., Johnson, K. M., Neill, C., Tilbrook, B., Towler, P., Inoue, H. Y., Ishii, M., and Shaffer, G.: The international at-sea intercomparison of fCO_2 systems during the R/V Meteor Cruise 36/1 in the North Atlantic Ocean, Marine Chemistry, 72, 171-192, 2000.

Lana, A., Bell, T., Simó, R., Vallina, S. M., Ballabrera-Poy, J., Kettle, A., Dachs, J., Bopp, L., Saltzman, E., and Stefels, J.: An updated climatology of surface dimethlysulfide concentrations and emission fluxes in the global ocean, Global Biogeochemical Cycles, 25, 2011.

Le Quéré, C., Andrew, R. M., Canadell, J. G., Sitch, S., Korsbakken, J. I., Peters, G. P., Manning, A. C., Boden, T. A., Tans, P. P., and Houghton, R. A.: Global carbon budget 2016, Earth System Science Data, 8, 605, 2016.

Liss, P. S., and Slater, P. G.: Flux of Gases across the Air-Sea Interface, Nature, 247, 181-184, 1974.

Loose, B., Stute, M., Alexander, P., and Smethie, W.: Design and deployment of a portable membrane equilibrator for sampling aqueous dissolved gases, Water Resources Research, 45, 2009.

Marandino, C. A., De Bruyn, W. J., Miller, S. D., and Saltzman, E. S.: Open ocean DMS air/sea fluxes over the eastern South Pacific Ocean, Atmos. Chem. Phys., 9, 345-356, 10.5194/acp-9-345-2009, 2009.

McNeil, C. L., and Merlivat, L.: The warm oceanic surface layer: Implications for CO_2 fluxes and surface gas measurements, Geophysical research letters, 23, 3575-3578, 1996.

Miller, S. D., Marandino, C., and Saltzman, E. S.: Ship-based measurement of air-sea CO_2 exchange by eddy covariance, Journal of Geophysical Research: Atmospheres, 115, 2010.

Millero, F. J., and Poisson, A.: International one-atmosphere equation of state of seawater, Deep Sea Research Part A. Oceanographic Research Papers, 28, 625-629, 1981.

Quinn, P., and Bates, T.: The case against climate regulation via oceanic phytoplankton sulphur emissions, Nature, 480, 51-56, 2011.

Ribas-Ribas, M., Rerolle, V., Bakker, D. C., Kitidis, V., Lee, G., Brown, I., Achterberg, E. P., Hardman-Mountford, N., and Tyrrell, T.: Intercomparison of carbonate chemistry measurements on a cruise in northwestern European shelf seas, Biogeosciences, 11, 4339-4355, 2014.

Ribas-Ribas, M., Mustaffa, N. I. H., Rahlff, J., Stolle, C., and Wurl, O.: Sea Surface Scanner (S3): A Catamaran for High-resolution Measurements of Biogeochemical Properties of the Sea Surface Microlayer, Journal of Atmospheric and Oceanic Technology, 2017.

Robertson, J. E., and Watson, A. J.: Thermal skin effect of the surface ocean and its implications for CO_2 uptake, Nature, 358, 738-740, 1992.

Royer, S.-J., Galí, M., Saltzman, E. S., McCormick, C. A., Bell, T. G., and Simó, R.: Development and validation of a shipboard system for measuring high-resolution vertical profiles of aqueous dimethylsulfide concentrations using chemical ionisation mass spectrometry, Environmental Chemistry, 11, 309-317, 2014.

Royer, S. J., Galí, M., Mahajan, A. S., Ross, O. N., Pérez, G. L., Saltzman, E. S., and Simó, R.: A high-resolution time-depth view of dimethylsulphide cycling in the surface sea, Scientific Reports, 6, 32325, 2016.

Saltzman, E. S., De Bruyn, W. J., Lawler, M., Marandino, C., and McCormick, C.: A chemical ionization mass spectrometer for continuous underway shipboard analysis of dimethylsulfide in near-surface seawater, Ocean Science, 5, 537-546, 2009.

Shutler, J. D., Land, P. E., Piolle, J.-F., Woolf, D. K., Goddijn-Murphy, L., Paul, F., Girard-Ardhuin, F., Chapron, B., and Donlon, C. J.: FluxEngine: A Flexible Processing System for Calculating Atmosphere–Ocean Carbon Dioxide Gas Fluxes and Climatologies, Journal of Atmospheric and Oceanic Technology, 33, 741-756, 2016.

Smyth, T., Pemberton, K., Aiken, J., and Geider, R.: A methodology to determine primary production and phytoplankton photosynthetic parameters from fast repetition rate fluorometry, Journal of Plankton Research, 26, 1337-1350, 2004.

Smyth, T. J., Fishwick, J. R., Lisa, A.-M., Cummings, D. G., Harris, C., Kitidis, V., Rees, A., Martinez-Vicente, V., and Woodward, E. M.: A broad spatio-temporal view of the Western English Channel observatory, Journal of Plankton Research, 32, 585-601, 2010.

Takahashi, T., Olafsson, J., Goddard, J. G., Chipman, D. W., and Sutherland, S.: Seasonal variation of CO_2 and nutrients in the high-latitude surface oceans: A comparative study, Global Biogeochemical Cycles, 7, 843-878, 1993.

Turk, D., Zappa, C. J., Meinen, C. S., Christian, J. R., Ho, D. T., Dickson, A. G., and McGillis, W. R.: Rain impacts on CO_2 exchange in the western equatorial Pacific Ocean, Geophysical Research Letters, 37, 2010.

Walker, C. F., Harvey, M. J., Smith, M. J., Bell, T. G., Saltzman, E. S., Marriner, A. S., McGregor, J. A., and Law, C. S.: Assessing the potential for dimethylsulfide enrichment at the sea surface and its influence on air-sea flux, Ocean Science, 12, 1033, 2016.

Wanninkhof, R.: Relationship between wind speed and gas exchange over the ocean revisited, Limnol. Oceanogr. Methods, 12, 351-362, 2014.

Ward, B., Wanninkhof, R., McGillis, W. R., Jessup, A. T., DeGrandpre, M. D., Hare, J. E., and Edson, J. B.: Biases in the air-sea flux of CO_2 resulting from ocean surface temperature gradients, Journal of Geophysical Research: Oceans (1978–2012), 109, 2004.

Webb, J. R., Maher, D. T., and Santos, I. R.: Automated, in situ measurements of dissolved CO_2, CH_4, and $\delta 13C$ values using cavity enhanced laser absorption spectrometry: Comparing response times of air-water equilibrators, Limnology and Oceanography: Methods, 14, 323-337, 2016.

Woolf, D., Land, P. E., Shutler, J. D., Goddijn-Murphy, L., and Donlon, C. J.: On the calculation of air-sea fluxes of CO_2 in the presence of temperature and salinity gradients, Journal of Geophysical Research: Oceans, 2016.

1 Yang, M., Beale, R., Smyth, T., and Blomquist, B.: Measurements of OVOC fluxes by eddy
2 covariance using a proton-transfer-reaction mass spectrometer–method development at a
3 coastal site, Atmospheric Chemistry and Physics, 13, 6165-6184, 2013.

4 Ziska, F., Quack, B., Abrahamsson, K., Archer, S., Atlas, E., Bell, T., Butler, J., Carpenter,
5 L., Jones, C., and Harris, N.: Global sea-to-air flux climatology for bromoform,
6 dibromomethane and methyl iodide, Atmospheric Chemistry and Physics, 13, 8915-8934,
7 2013.